

Nuclear energy density functional from chiral pion-nucleon dynamics¹

N. Kaiser^a, S. Fritsch^a and W. Weise^{a,b}

^a Physik Department, Technische Universität München, D-85747 Garching, Germany

^b ECT*, I-38050 Villazzano (Trento), Italy

email: nkaiser@physik.tu-muenchen.de

Abstract

We calculate the nuclear energy density functional relevant for $N=Z$ even-even nuclei in the systematic framework of chiral perturbation theory. The calculation includes the one-pion exchange Fock diagram and the iterated one-pion exchange Hartree and Fock diagrams. From these few leading order contributions in the small momentum expansion one obtains already a very good equation of state of isospin symmetric nuclear matter. We find that in the region below nuclear matter saturation density the effective nucleon mass $\widetilde{M}^*(\rho)$ deviates by at most 15% from its free space value M , with $0.89M < \widetilde{M}^*(\rho) < M$ for $\rho < 0.11 \text{ fm}^{-3}$ and $\widetilde{M}^*(\rho) > M$ for higher densities. The parameterfree strength of the $(\vec{\nabla}\rho)^2$ -term, $F_{\nabla}(k_f)$, is at saturation density comparable to that of phenomenological Skyrme forces. The magnitude of $F_J(k_f)$ accompanying the squared spin-orbit density \vec{J}^2 comes out somewhat larger. The strength of the nuclear spin-orbit interaction, $F_{so}(k_f)$, as given by iterated one-pion exchange is about half as large as the corresponding empirical value, however, with the wrong negative sign. The novel density dependencies of $\widetilde{M}^*(\rho)$ and $F_{\nabla,so,J}(k_f)$ as predicted by our parameterfree calculation should be examined in nuclear structure calculations (after introducing an additional short range spin-orbit contribution constant in density).

PACS: 12.38.Bx, 21.30.Fe, 21.60.-n, 31.15.Ew

Keywords: Nuclear energy density functional; Density-matrix expansion; Perturbative chiral pion-nucleon dynamics

1 Introduction

Among the various phenomenological interactions that have been used extensively in the description of nuclei, the Skyrme force [1] has gained much popularity because of its analytical simplicity and its ability to reproduce nuclear properties over the whole periodic table within the self-consistent Hartree-Fock approximation. Several Skyrme parameterizations have been tailored to account for single particle spectra [2], giant monopole resonances [3] or fission barriers of heavy nuclei [4]. Recently, a new Skyrme force which also reproduces the equation of state of pure neutron matter up to neutron star densities, $\rho_n \simeq 1.5 \text{ fm}^{-3}$, has been proposed in ref.[5] for the study of nuclei far from stability. A microscopic interpretation of the various parameters entering the effective Skyrme forces is generally put aside. Sometimes the energy density functional is just parameterized without reference to any effective (zero-range) two-body interaction in order to avoid the complete fixing of time-reversal-odd terms by the Pauli-exclusion principle [6].

¹Work supported in part by BMBF, GSI and DFG.

Another widely and successfully used approach to nuclear structure calculations are relativistic mean-field models [7]. In these models the nucleus is described as a collection of independent Dirac-particles moving in self-consistently generated scalar and vector mean-fields. The footprints of relativity become visible through the large nuclear spin-orbit interaction which emerges in that framework naturally from the interplay of the two strong and counteracting (scalar and vector) mean-fields. The corresponding many-body calculations are usually carried out in the Hartree approximation, ignoring the negative-energy Dirac-sea. For a recent review on self-consistent mean-field models for nuclear structure, see ref.[6]. In that article the relationship between the relativistic mean-field models and the Skyrme phenomenology is also discussed.

The first conditions to be fulfilled by any phenomenological nucleon-nucleon interaction come from the (few empirically known) properties of infinite nuclear matter. These are the saturation density $\rho_0 = 2k_{f0}^3/3\pi^2$, the binding energy per particle $-\bar{E}(k_{f0})$ and the compression modulus $K = k_{f0}^2\bar{E}''(k_{f0})$ of isospin symmetric nuclear matter as well as the asymmetry energy $A(k_{f0})$. In general, Skyrme forces involve several more parameters related to terms in the energy density functional which vanish identically in homogeneous nuclear matter (like the spin-orbit coupling proportional to the density-gradient).

In a recent work [8], we have used chiral perturbation theory for a systematic treatment of the nuclear matter many-body problem. In this calculation the contributions to the energy per particle, $\bar{E}(k_f)$, originate exclusively from one- and two-pion exchange between nucleons and they are ordered in powers of the Fermi momentum k_f (modulo functions of k_f/m_π). It has been demonstrated in ref.[8] that the empirical saturation point ($\rho_0 \simeq 0.17 \text{ fm}^{-3}$, $\bar{E}(k_{f0}) \simeq -15.3 \text{ MeV}$) and the nuclear matter compressibility $K \simeq 255 \text{ MeV}$ can be well reproduced at order $\mathcal{O}(k_f^5)$ in the small momentum expansion with just one single momentum cut-off scale of $\Lambda \simeq 0.65 \text{ GeV}$ which parameterizes the necessary short range NN-dynamics. Most surprisingly, the prediction for the asymmetry energy, $A(k_{f0}) = 33.8 \text{ MeV}$, is in very good agreement with its empirical value. Furthermore, as a nontrivial fact, pure neutron matter is predicted to be unbound and the corresponding equation of state $\bar{E}_n(k_n)$ agrees roughly with that of sophisticated many-body calculations for low neutron densities $\rho_n \leq 0.25 \text{ fm}^{-3}$. In a subsequent work [9], the momentum and density dependent (real) single-particle potential $U(p, k_f)$ has been calculated in the same framework. It was found that chiral 1π - and 2π -exchange give rise to a potential depth for a nucleon at the bottom of the Fermi sea of $U(0, k_{f0}) = -53.2 \text{ MeV}$. This value is in very good agreement with the depth of the empirical optical model potential and the nuclear shell model potential. In fact very similar results for nuclear matter can be obtained already at order $\mathcal{O}(k_f^4)$ in the small momentum expansion (by dropping the relativistic $1/M^2$ -correction to 1π -exchange and the irreducible 2π -exchange of order $\mathcal{O}(k_f^5)$) with a somewhat reduced cut-off scale of $\Lambda \simeq 0.61 \text{ GeV}$. Detailed results of this $\mathcal{O}(k_f^4)$ -calculation can be found in ref.[10] (it is named "mean-field treatment of the NN-contact interaction" therein).

Given the fact that many properties of nuclear matter can be well described by chiral πN -dynamics treated perturbatively up to three-loop order it is natural to consider in a further step the energy density functional relevant for inhomogeneous many-nucleon systems (i.e. finite nuclei). We will restrict ourselves here to the isospin symmetric case of equal proton and neutron number $N=Z$. The aim of this work is to calculate density-dependent generalizations of those combinations of Skyrme parameters which belong to terms specific for the inhomogeneous many-nucleon system, such as $(\vec{\nabla}\rho)^2$. This novel density-dependence is a consequence of the finite range character of the 1π - and 2π -exchange interaction. We stress already here that our results for the density-dependent strength functions are completely parameterfree. In particular, they are independent of the cut-off scale Λ adjusted in ref.[8, 10] to the binding energy per particle $-\bar{E}(k_{f0}) = 15.3 \text{ MeV}$.

Our paper is organized as follows. In the next section we recall the essential results of the density-matrix expansion of Negele and Vautherin [11] which provides the adequate technical

framework to compute the nuclear energy density functional. In section 3, we then present analytical formulas for the various strength functions $F_\tau(k_f)$, $F_d(k_f)$, $F_{so}(k_f)$ and $F_J(k_f)$ entering the nuclear energy density functional. These expressions are derived (exclusively) from the two-loop 1π -exchange Fock diagram and the three-loop iterated 1π -exchange Hartree and Fock diagrams. Section 4 is devoted to a discussion of our results and finally section 5 ends with a summary and an outlook.

2 Density-matrix expansion and energy density functional

The starting point for the construction of an explicit nuclear energy density functional is the density-matrix as given by a sum over the occupied energy eigenfunctions Ψ_α of this many-fermion system. According to Negele and Vautherin [11] the bilocal density-matrix can be expanded in relative and center-of-mass coordinates, \vec{a} and \vec{r} , as follows:

$$\sum_{\alpha \in occ} \Psi_\alpha(\vec{r} - \vec{a}/2) \Psi_\alpha^\dagger(\vec{r} + \vec{a}/2) = \frac{3\rho}{ak_f} j_1(ak_f) - \frac{35}{2ak_f^3} j_3(ak_f) \left[\tau - \frac{3}{5} \rho k_f^2 - \frac{1}{4} \vec{\nabla}^2 \rho \right] + \frac{i}{2} j_0(ak_f) \vec{\sigma} \cdot (\vec{a} \times \vec{J}) + \dots, \quad (1)$$

where the functions $j_l(ak_f)$ are ordinary spherical Bessel functions. The other quantities appearing on the right hand side of eq.(1) are the local nucleon density:

$$\rho(\vec{r}) = \frac{2k_f^3(\vec{r})}{3\pi^2} = \sum_{\alpha \in occ} \Psi_\alpha^\dagger(\vec{r}) \Psi_\alpha(\vec{r}), \quad (2)$$

written here in terms of the local Fermi-momentum $k_f(\vec{r})$, the local kinetic energy density:

$$\tau(\vec{r}) = \sum_{\alpha \in occ} \vec{\nabla} \Psi_\alpha^\dagger(\vec{r}) \cdot \vec{\nabla} \Psi_\alpha(\vec{r}), \quad (3)$$

and the local spin-orbit density:

$$\vec{J}(\vec{r}) = \sum_{\alpha \in occ} \Psi_\alpha^\dagger(\vec{r}) i \vec{\sigma} \times \vec{\nabla} \Psi_\alpha(\vec{r}). \quad (4)$$

For notational simplicity we have dropped their argument \vec{r} in eq.(1) and will do so in the following. It is important to note that a pairwise filling of time-reversed orbitals α has been assumed in eq.(1). If the many-body ground state is not time-reversal invariant (as it is the case for odd nuclei and for rotating nuclei) various additional time-reversal-odd fields come into play [6]. The local spin-orbit density $\vec{J}(\vec{r})$ is non-zero for spin-unsaturated shells. In such a situation the density-matrix is no longer a scalar in spin-space but has also a vector part. The Fourier transform of the density-matrix eq.(1) with respect to both coordinates \vec{a} and \vec{r} defines the medium insertion for the inhomogeneous many-nucleon system characterized by the time-reversal-even fields $\rho(\vec{r})$, $\tau(\vec{r})$ and $\vec{J}(\vec{r})$:

$$\Gamma(\vec{p}, \vec{q}) = \int d^3r e^{-i\vec{q}\cdot\vec{r}} \left\{ \theta(k_f - |\vec{p}|) \left[1 + \frac{35\pi^2}{8k_f^7} (5\vec{p}^2 - 3k_f^2) \left(\tau - \frac{3}{5} \rho k_f^2 - \frac{1}{4} \vec{\nabla}^2 \rho \right) \right] + \frac{\pi^2}{4k_f^4} \left[\delta(k_f - |\vec{p}|) - k_f \delta'(k_f - |\vec{p}|) \right] \vec{\sigma} \cdot (\vec{p} \times \vec{J}) \right\}. \quad (5)$$

The double line in the left picture of Fig.1 symbolizes this medium insertion together with the assignment of the out- and in-going nucleon momenta $\vec{p} \pm \vec{q}/2$. The momentum transfer \vec{q} is

provided by the Fourier components of the inhomogeneous (matter) distributions: $\rho(\vec{r})$, $\tau(\vec{r})$ and $\vec{J}(\vec{r})$. As a check one verifies that the Fourier transform $(1/2\pi^3) \int d^3p e^{-i\vec{p}\cdot\vec{a}}$ of the (partly very singular) expression in the curly brackets in eq.(5) gives exactly the right hand side of the density-matrix expansion in eq.(1). For homogeneous nuclear matter (where $\tau = 3\rho k_f^2/5$ and $\vec{\nabla}\rho = \vec{J} = \vec{0}$) only the familiar step-function $\theta(k_f - |\vec{p}|)$ remains from the medium insertion eq.(5) as the density of nucleon states in momentum space.

Going up to second order in spatial gradients (i.e. deviations from homogeneity) the energy density functional relevant for N=Z even-even nuclei reads [12]:

$$\begin{aligned} \mathcal{E}[\rho, \tau, \vec{J}] = & \rho \bar{E}(k_f) + \left[\tau - \frac{3}{5}\rho k_f^2 \right] \left[\frac{1}{2M} - \frac{5k_f^2}{56M^3} + F_\tau(k_f) \right] \\ & + (\vec{\nabla}\rho)^2 F_\nabla(k_f) + \vec{\nabla}\rho \cdot \vec{J} F_{so}(k_f) + \vec{J}^2 F_J(k_f). \end{aligned} \quad (6)$$

Here, $\bar{E}(k_f)$ is the energy per particle of isospin symmetric nuclear matter evaluated at the local Fermi momentum $k_f(\vec{r})$. The (small) relativistic correction term $-5k_f^2/56M^3$ has been included in eq.(6) for the following reason. When multiplied with $-3\rho k_f^2/5$ it cancels together with the foregoing term $1/2M$ the relativistically improved kinetic energy in $\bar{E}(k_f)$ (see eq.(5) in ref.[8]). The functions $F_\tau(k_f)$, $F_\nabla(k_f)$, $F_{so}(k_f)$ and $F_J(k_f)$ arising from NN-interactions encode new dynamical information specific for inhomogeneous many-nucleon systems. In Skyrme parameterizations $F_\tau(k_f)$ depends linearly on the (local) density $\rho = 2k_f^3/3\pi^2$ whereas $F_{\nabla,so,J}(k_f)$ are just constants. Note that $F_{so}(k_f)$ gives the strength of the nuclear spin-orbit coupling while $F_\nabla(k_f)$ is responsible for the formation of the nuclear surface. Variation of the energy density functional $\mathcal{E}[\rho, \tau, \vec{J}]$ with respect to single-particle wavefunctions under the condition that these are normalized to unity leads to self-consistent density dependent Hartree-Fock equations [12].

Returning to the medium insertion in eq.(5) one sees that the strength function $F_\tau(k_f)$ emerges via a perturbation on top of the density of states $\theta(k_f - |\vec{p}|)$. The single particle potential in nuclear matter can actually be constructed in the same way by introducing a delta-function like perturbation [9]. Consequently, the strength function $F_\tau(k_f)$ can be directly expressed in terms of the real part $U(p, k_f)$ of the momentum and density dependent single particle potential as:

$$F_\tau(k_f) = \frac{35}{4k_f^7} \int_0^{k_f} dp p^2 (5p^2 - 3k_f^2) U(p, k_f). \quad (7)$$

In eq.(5) the term $\tau - 3\rho k_f^2/5$ is accompanied by $-\vec{\nabla}^2\rho/4$. Performing a partial integration of the energy $\int d^3r \mathcal{E}$ one sees immediately that part of the strength function $F_\nabla(k_f)$ is given by the ρ -derivative of $F_\tau(k_f)/4$. These considerations lead to the following decomposition:

$$F_\nabla(k_f) = \frac{\pi^2}{8k_f^2} \frac{\partial F_\tau(k_f)}{\partial k_f} + F_d(k_f), \quad (8)$$

where $F_d(k_f)$ comprises all those contributions for which the $(\vec{\nabla}\rho)^2$ -factor originates directly from the interactions. An example for this mechanism will be explained in the next section.

As a check on the present formalism (summarized in eq.(5)) we rederived the Skyrme energy density functional (eq.(5.87) in ref.[12]) from the matrix elements of the underlying two-body potential (eq.(4.105) in ref.[12]) in a purely diagrammatic framework. In the next section we use the same formalism to compute the nuclear energy density functional eq.(6) from one- and two-pion exchange diagrams.

3 Diagrammatic calculation

In this section we present analytical formulas for the four strength functions $F_\tau(k_f)$, $F_d(k_f)$, $F_{so}(k_f)$ and $F_J(k_f)$ as derived from the two-loop one-pion exchange Fock diagram and the three-loop iterated one-pion exchange Hartree and Fock diagrams. These graphs are shown in Fig.1. We give for each diagram only the final result omitting all technical details related to extensive algebraic manipulations and solving elementary integrals.

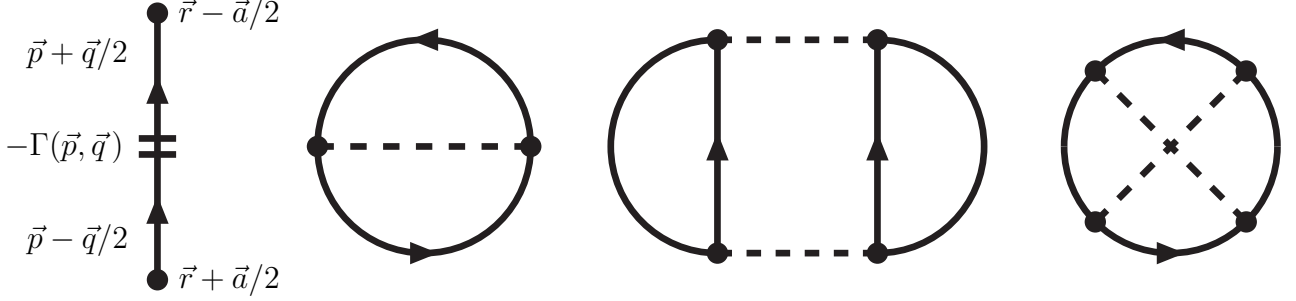


Fig. 1: Left: The double line symbolizes the medium insertion defined by eq.(5). Next are shown: The two-loop one-pion exchange Fock-diagram and the three-loop iterated one-pion exchange Hartree- and Fock-diagrams. The combinatoric factors of these diagrams are $1/2$, $1/4$ and $1/4$, in the order shown. Their isospin factors for isospin symmetric nuclear matter are 6 , 12 and -6 , respectively.

3.1 One-pion exchange Fock diagram with two medium insertions

The non-vanishing contributions read:

$$F_\tau(k_f) = \frac{35g_A^2 m_\pi}{(16\pi f_\pi)^2 u^5} \left\{ \frac{4}{3} u^4 + 24u^2 - 1 - 20u \arctan 2u + \left(\frac{9}{2} - 6u^2 + \frac{1}{4u^2} \right) \ln(1 + 4u^2) \right\}, \quad (9)$$

$$F_J(k_f) = \frac{g_A^2}{(8m_\pi f_\pi)^2} \left\{ \frac{10 + 24u^2}{(1 + 4u^2)^2} + \frac{1}{2u^2} \ln(1 + 4u^2) \right\}, \quad (10)$$

with $u = k_f/m_\pi$ the ratio of the two small scales inherent to our calculation. The expression for $F_\tau(k_f)$ in eq.(9) follows simply from inserting the static 1π -exchange single particle potential (eq.(8) in ref.[9] in the limit $M \rightarrow \infty$) into the "master formula" eq.(7). The vanishing of $F_d(k_f)$ has the following reason. The momentum transfer $\pm\vec{q}$ at the upper and lower medium insertion does not flow into the exchanged virtual pion line (because of momentum conservation at each interaction vertex). Therefore there is no factor of \vec{q}^2 which could produce via Fourier transformations a $(\vec{\nabla}\rho)^2$ -factor. The spin-orbit strength $F_{so}(k_f)$ vanishes as a result of the spin-trace: $\text{tr}[\vec{\sigma} \cdot (\vec{p}_1 - \vec{p}_2) \vec{\sigma} \cdot (\vec{p}_{1,2} \times \vec{J}) \vec{\sigma} \cdot (\vec{p}_1 - \vec{p}_2)] = 0$.

3.2 Iterated one-pion exchange Hartree diagram with two medium insertions

We find the following closed form expressions:

$$F_\tau(k_f) = \frac{g_A^4 M m_\pi^2}{(8\pi)^3 (u f_\pi)^4} \left\{ \frac{151}{3} u^3 - (350 + 16u^4) \arctan 2u + 444u - \frac{55}{4u} + \left(\frac{55}{16u^3} + \frac{567}{8u} - \frac{245}{2} u \right) \ln(1 + 4u^2) \right\}, \quad (11)$$

$$F_d(k_f) = \frac{g_A^4 M}{\pi m_\pi (4f_\pi)^4} \left\{ \frac{4}{u} \arctan 2u - \frac{23}{16u^2} \ln(1 + 4u^2) - \frac{3 + 20u^2}{12(1 + 4u^2)^2} \right\}, \quad (12)$$

$$F_{so}(k_f) = \frac{g_A^4 M}{\pi m_\pi (4f_\pi)^4} \left\{ \frac{4}{1 + 4u^2} - \frac{3}{2u^2} \ln(1 + 4u^2) \right\}. \quad (13)$$

Again, $F_\tau(k_f)$ in eq.(11) stems from inserting the two-body potential $U_2(p, k_f)$ (eq.(9) in ref.[9]) into the "master formula" eq.(7). Note that any p -independent contribution, in particular the cut-off dependent term eq.(17) in ref.[9], drops out. The vanishing of $F_J(k_f)$ results from the spin-trace over a nucleon ring being equal to zero (as demonstrated at the end of section 3.1). Let us briefly explain the mechanism which generates the strength function $F_d(k_f)$. The exchanged pion-pair transfers the momentum \vec{q} between the left and the right nucleon ring. This momentum \vec{q} enters both the pseudovector πN -interaction vertices and the pion propagators. After expanding the inner loop integral to order \vec{q}^2 the Fourier transformation in eq.(5) converts this factor \vec{q}^2 into a factor $(\vec{\nabla} k_f)^2$. The rest is a solvable integral over the product of two Fermi surfaces. The spin-orbit strength $F_{so}(k_f)$ arises from the spin-trace: $\text{tr}[\vec{\sigma} \cdot (\vec{l} + \vec{q}/2) \vec{\sigma} \cdot (\vec{l} - \vec{q}/2) \vec{\sigma} \cdot (\vec{p}_{1,2} \times \vec{J})] = 2i (\vec{q} \times \vec{l}) \cdot (\vec{p}_{1,2} \times \vec{J})$ where \vec{q} gets again converted to $\vec{\nabla} k_f$ by Fourier transformation. The remainder is a solvable integral over delta-functions and derivatives thereof.

3.3 Iterated one-pion exchange Fock diagram with two medium insertions

We find the following contributions from the last diagram in Fig. 1 with two medium insertions at non-neighboring nucleon propagators:

$$F_\tau(k_f) = \frac{35g_A^4 M m_\pi^2}{(4\pi)^3 f_\pi^4 u^7} \int_0^u dx \frac{x^2(u-x)^2}{2(1+2x^2)} (2x^2 + 4ux - 3u^2) \\ \times \left[(1 + 8x^2 + 8x^4) \arctan x - (1 + 4x^2) \arctan 2x \right], \quad (14)$$

$$F_d(k_f) = \frac{g_A^4 M}{\pi m_\pi (8f_\pi)^4} \left\{ \frac{4}{u} (\arctan u - 2 \arctan 2u) + \frac{1}{u^2} \ln \frac{(1 + 2u^2)(1 + 4u^2)}{(1 + u^2)^2} \right. \\ \left. + \frac{4}{1 + 2u^2} + \frac{2}{u^2} \int_0^u dx \frac{3 + 18x^2 + 16x^4}{(1 + 2x^2)^3} [\arctan 2x - \arctan x] \right\}, \quad (15)$$

$$F_{so}(k_f) = \frac{g_A^4 M}{\pi m_\pi (4f_\pi)^4} \left\{ \frac{1}{4u^2} \ln \frac{1 + 4u^2}{1 + u^2} + \frac{3 + 4u^2}{2u(1 + 2u^2)} \arctan u \right. \\ \left. - \frac{\arctan 2u}{2u(1 + 2u^2)} + \frac{1}{2u^2} \int_0^u dx \frac{\arctan x - \arctan 2x}{1 + 2x^2} \right\}, \quad (16)$$

$$F_J(k_f) = \frac{g_A^4 M}{\pi m_\pi (8f_\pi)^4} \left\{ \frac{2 \arctan 2u}{u(1 + 2u^2)} - \frac{2(5 + 8u^2)}{u(1 + 2u^2)} \arctan u - \frac{1}{1 + u^2} \right. \\ \left. - \frac{1}{u^2} \ln \frac{1 + 4u^2}{1 + u^2} + \frac{2}{u^2} \int_0^u dx \frac{\arctan 2x - \arctan x}{1 + 2x^2} \right\}. \quad (17)$$

The basic mechanisms which lead to these results are the same as explained before. Concerning kinematics and spin-algebra the iterated 1π -exchange Fock diagram is somewhat more involved than the Hartree diagram. Even though all occurring inner d^3l -loop integrals can be solved in closed form there remain some non-elementary integrals from the integration over the product of two Fermi spheres of radius k_f .

3.4 Iterated one-pion exchange Hartree diagram with three medium insertions

In this case we find the following contributions:

$$\begin{aligned}
F_\tau(k_f) &= \frac{175g_A^4 M m_\pi^2}{(4\pi f_\pi)^4 u^7} \int_0^u dx x^2 \int_{-1}^1 dy \left\{ u^3 xy \left[\ln(1+s^2) - \frac{2s^2+s^4}{2(1+s^2)} \right] + [2uxy + (u^2 - x^2 y^2)H] \right. \\
&\times \left[\frac{3}{4} \left(3 + \frac{13}{5} u^2 - 4x^2 - x^2 y^2 \right) \ln(1+s^2) + \left(4x^2 + x^2 y^2 - \frac{13}{5} u^2 - 2 \right) \frac{3(2s^2+s^4)}{8(1+s^2)} \right. \\
&\left. \left. + \frac{3}{8} s^2 (s^2 - 2) + sxy(6 - s^2) + \frac{3sxy}{2(1+s^2)} - \frac{15}{2} xy \arctan s \right] \right\}, \quad (18)
\end{aligned}$$

with the auxiliary functions $H = \ln(u + xy) - \ln(u - xy)$ and $s = xy + \sqrt{u^2 - x^2 + x^2 y^2}$. The quantity s has the geometrical meaning of the distance between a point on a sphere of radius u and an interior point displaced at a distance x from the center of the sphere. In the same geometrical picture y denotes a directional cosine.

$$\begin{aligned}
F_d(k_f) &= \frac{g_A^4 M u^{-4}}{\pi^2 m_\pi (4f_\pi)^4} \int_0^u dx x^2 \int_{-1}^1 dy \left\{ H \left[\frac{s^2}{4(1+s^2)^4} (7s^6 + 38s^4 + 63s^2 + 24) \right. \right. \\
&\left. \left. - 6 \ln(1+s^2) \right] + \frac{uxy}{u^2 - x^2 y^2} \left[\frac{s^2}{6(1+s^2)^3} (23s^4 + 51s^2 + 24) - 4 \ln(1+s^2) \right] \right\}, \quad (19)
\end{aligned}$$

$$\begin{aligned}
F_{so}(k_f) &= \frac{2g_A^4 M u^{-6}}{\pi^2 m_\pi (4f_\pi)^4} \int_0^u dx x^2 \int_{-1}^1 dy \left\{ \frac{2us^4 [2x^2 y^2 (s - s') - u^2 s]}{(1+s^2)^2 (u^2 - x^2 y^2)} \right. \\
&+ \left[\frac{u(3u^2 - 5x^2 y^2)}{u^2 - x^2 y^2} - 4xyH \right] \left[3 \arctan s - \frac{3s + 2s^3}{1+s^2} \right] + \frac{H s^4}{(1+s^2)^3} \\
&\left. \times \left[(5 + s^2) s'^2 - 2xys'(7 + 3s^2) + sxy(11 + 7s^2) + (s + s^3)(s'' - s') \right] \right\}. \quad (20)
\end{aligned}$$

Here we have introduced the partial derivatives $s' = u \partial s / \partial u$ and $s'' = u^2 \partial^2 s / \partial u^2$.

$$\begin{aligned}
F_J(k_f) &= \frac{g_A^4 M}{\pi^2 m_\pi (4f_\pi)^4} \left\{ \frac{96u^6 + 24u^4 - 12u^2 - 1}{u(1+4u^2)^3} + \frac{1+2u^2}{4u^3} \ln(1+4u^2) + \int_0^1 dy \frac{8u^3 y^2}{(1+4u^2 y^2)^4} \right. \\
&\left. \times \left[(30 + 32u^2) y^2 - 5 + (16u^4 - 24u^2 - 35) y^4 - 56u^2 y^6 - 48u^4 y^8 \right] \ln \frac{1+y}{1-y} \right\}. \quad (21)
\end{aligned}$$

The last contribution $F_J(k_f)$ in eq.(21) is obtained when both insertions proportional to $\vec{\sigma} \cdot (\vec{p}_{1,2} \times \vec{J})$ (producing, after integration, the overall \vec{J}^2 -factor) are under a single spin-trace. For the other two possible combinations the spin-traces are equal to zero.

3.5 Iterated one-pion exchange Fock diagram with three medium insertions

The evaluation of this diagram is most tedious. It is advisable to split the contributions to the four strength functions $F_\tau(k_f)$, $F_d(k_f)$, $F_{so}(k_f)$ and $F_J(k_f)$ into "factorizable" and "non-factorizable" parts. These two pieces are distinguished by whether the nucleon propagator in the denominator can be canceled or not by terms from the product of πN -interaction vertices in the numerator.

We find the following "factorizable" contributions:

$$\begin{aligned}
F_\tau(k_f) &= \frac{35g_A^4 M m_\pi^2}{2(8\pi f_\pi)^4 u^7} \int_0^u dx \left[u(1+u^2+x^2) - [1+(u+x)^2][1+(u-x)^2]L \right] \\
&\times \left\{ 5u(5x^4+19x^2-2) - u^3\left(\frac{26}{3}x^2+17\right) - 7u^5 \right. \\
&- 80x^2 \left[\arctan(u+x) + \arctan(u-x) \right] + [(1+u^2)^2(10+7u^2) \\
&\left. + 3x^2(25+8u^2-13u^4) + 3x^4(19u^2-40) - 25x^6 \right] L \left. \right\}, \tag{22}
\end{aligned}$$

with the auxiliary function:

$$L = \frac{1}{4x} \ln \frac{1+(u+x)^2}{1+(u-x)^2}, \tag{23}$$

$$\begin{aligned}
F_d(k_f) &= \frac{g_A^4 M u^{-2}}{\pi^2 m_\pi (8f_\pi)^4} \left\{ \frac{1+6u^2}{4u^3} \ln^2(1+4u^2) - \frac{5+52u^2+104u^4}{2u(1+u^2)(1+4u^2)} \ln(1+4u^2) \right. \\
&- \frac{19u^2}{1+u^2} \arctan 2u + \frac{6u(1+8u^2)}{1+4u^2} + 8 \int_0^u dx \left\{ [1+u^2+3(1+u^2)^2x^{-2}]L^2 \right. \\
&+ 3u^2x^{-2} + [(4u-x)[1+(u+x)^2]^{-1} + (4u+x)[1+(u-x)^2]^{-1} \\
&\left. - 4u - 6(u+u^3)x^{-2} - 2x[1+(u+x)^2]^{-2} + 2x[1+(u-x)^2]^{-2} \right\} L \left. \right\}, \tag{24}
\end{aligned}$$

$$\begin{aligned}
F_{so}(k_f) &= \frac{g_A^4 M u^{-3}}{\pi^2 m_\pi (4f_\pi)^4} \left\{ \frac{1+2u^2}{32u^2} \ln^2(1+4u^2) - \frac{3u^4 \ln(1+4u^2)}{(1+u^2)(1+4u^2)} + \frac{u^2(3+20u^2)}{2(1+4u^2)} \right. \\
&- \frac{u(1+11u^2+16u^4)}{(1+u^2)(1+4u^2)} \arctan 2u + \int_0^u dx \left\{ [3(1+u^2)^2x^{-2} - 4x^2 - 1 - u^2]uL^2 \right. \\
&+ [(1+5u^2+5ux)[1+(u+x)^2]^{-1} + (1+5u^2-5ux)[1+(u-x)^2]^{-1} \\
&\left. - 6(u^2+u^4)x^{-2} - 2 \right] L + 3u^3x^{-2} \left. \right\}, \tag{25}
\end{aligned}$$

$$\begin{aligned}
F_J(k_f) &= \frac{g_A^4 M u^{-3}}{\pi^2 m_\pi (8f_\pi)^4} \left\{ \frac{3+12u^2+8u^4}{4u^4} \ln^2(1+4u^2) - \frac{7+8u^2+8u^4}{u^2(1+u^2)} \ln(1+4u^2) \right. \\
&+ \frac{2(5-2u^2)(2+3u^2)}{u(1+u^2)} \arctan 2u + \frac{8(8u^6-158u^4-73u^2-9)}{3(1+4u^2)^2} \\
&+ 8 \int_0^u dx \left\{ [3(1+u^2)^2x^{-2} + 3x^2 - 2 - 2u^2]uL^2 + 2[2+u^2-3x^{-2}(u^2+u^4) \right. \\
&\left. + (u^2-ux-1)[1+(u+x)^2]^{-1} + (u^2+ux-1)[1+(u-x)^2]^{-1} \right\} L + 3u^3x^{-2} \left. \right\}. \tag{26}
\end{aligned}$$

The "non-factorizable" contributions read on the other hand:

$$\begin{aligned}
F_\tau(k_f) &= \frac{35g_A^4 M m_\pi^2}{(8\pi f_\pi)^4 u^7} \int_0^u dx x^2 \int_{-1}^1 dy \int_{-1}^1 dz \frac{yz \theta(y^2+z^2-1)}{|yz|\sqrt{y^2+z^2-1}} \\
&\times \left[t^2 - \ln(1+t^2) \right] \left\{ (45x^2-27u^2-30) \ln(1+s^2) \right. \\
&\left. + 120xy \arctan s + 2sxy(17u^2-30-35x^2+20x^2y^2) \right\}, \tag{27}
\end{aligned}$$

$$\begin{aligned}
F_d(k_f) &= \frac{g_A^4 M u^{-6}}{\pi^2 m_\pi (8f_\pi)^4} \int_0^u dx x^2 \int_{-1}^1 dy \int_{-1}^1 dz \frac{yz \theta(y^2 + z^2 - 1)}{|yz| \sqrt{y^2 + z^2 - 1}} \left\{ \left[2 \ln(1 + t^2) - \frac{t^2(3 + t^2)}{(1 + t^2)^2} \right] \right. \\
&\quad \left. \times \frac{2s^2}{(1 + s^2)^2} \left[(6s + 4s^3)s' - (3 + s^2)s'^2 - (s + s^3)s'' \right] + \frac{4s^3 s' t^2 (2t^4 + 5t^2 - 1)}{(1 + s^2)(1 + t^2)^3} \right\}, \quad (28)
\end{aligned}$$

$$\begin{aligned}
F_{so}(k_f) &= \frac{g_A^4 M}{\pi^2 m_\pi (4f_\pi)^4} \int_{-1}^1 dy \int_{-1}^1 dz \frac{yz \theta(y^2 + z^2 - 1)}{|yz| \sqrt{y^2 + z^2 - 1}} \left\{ 16y^2 z \theta(y) \theta(z) \left[\frac{1 + 2u^2 y^2}{(1 + 4u^2 y^2)^2} \right. \right. \\
&\quad \left. \left. \times \left(\arctan 2uz - 2uz \right) + \frac{u^3 z (1 - 2z^2)}{(1 + 4u^2 y^2)(1 + 4u^2 z^2)} \right] + \int_0^u dx \frac{u^{-8} x^2 s t^2 t'}{2(1 + s^2)^2 (1 + t^2)} \right. \\
&\quad \left. \times \left[(s + s^3)(s' - s'')(st + sxz - txy) + s'^2(2txy - (3s + s^3)(t + xz)) \right] \right\}, \quad (29)
\end{aligned}$$

$$\begin{aligned}
F_J(k_f) &= \frac{g_A^4 M}{\pi^2 m_\pi (4f_\pi)^4} \int_{-1}^1 dy \int_{-1}^1 dz \frac{yz \theta(y^2 + z^2 - 1)}{|yz| \sqrt{y^2 + z^2 - 1}} \left\{ y^2 \theta(y) \theta(z) \left[\ln(1 + 4u^2 z^2) - 4u^2 z^2 \right] \right. \\
&\quad \left. \times \frac{9 + 4u^2(5 + 2y^2) + 16u^4(y^2 + y^4)}{u(1 + 4u^2 y^2)^3} + \frac{16u^3(3 + 4u^2 y^2)z^2(1 - 2z^2)}{(1 + 4u^2 y^2)^2(1 + 4u^2 z^2)} \right] \\
&\quad + \int_0^u dx \frac{x^4 s^2 t^2 (1 - y^2 - z^2)}{4u^{10}(1 + s^2)^2(1 + t^2)^2} \left[(s + s^3)(s'' - s') + (3 + s^2)s'^2 \right] \\
&\quad \left. \times \left[(t + t^3)(t'' - t') + (3 + t^2)t'^2 \right] \right\}, \quad (30)
\end{aligned}$$

with the auxiliary function $t = xz + \sqrt{u^2 - x^2 + x^2 z^2}$ and its partial derivatives $t' = u \partial t / \partial u$ and $t'' = u^2 \partial^2 t / \partial u^2$. For the numerical evaluation of the $dydz$ -double integrals in eqs.(27-30) it is advantageous to first antisymmetrize the integrands both in y and z and then to substitute $z = \sqrt{y^2 \zeta^2 + 1 - y^2}$. This way the integration region becomes equal to the unit-square $0 < y, \zeta < 1$.

Obviously, the analytical results presented in this section do not involve any adjustable parameter. Only well-known physical quantities like the nucleon axial-vector coupling constant $g_A = 1.3$, the nucleon mass $M = 939$ MeV, the pion decay constant $f_\pi = 92.4$ MeV and the (neutral) pion mass $m_\pi = 135$ MeV enter.

Let us end this section with general power counting considerations for the nuclear energy density functional $\mathcal{E}[\rho, \tau, \vec{J}]$. Counting the Fermi momentum k_f , the pion mass m_π and a spatial gradient $\vec{\nabla}$ collectively as small momenta one deduces from eqs.(2,3,4) that the nucleon density $\rho(\vec{r})$, the kinetic energy density $\tau(\vec{r})$ and the spin-orbit density $\vec{J}(\vec{r})$ are quantities of third, fifth and fourth order in small momenta, respectively. With these counting rules the contributions from 1π -exchange to the nuclear energy density functional $\mathcal{E}[\rho, \tau, \vec{J}]$ are of sixth order in small momenta while all contributions from iterated 1π -exchange are of seventh order. Concerning NN-interactions induced by pion-exchange the nuclear energy density functional presented here is in fact complete up-to-and-including seventh order in small momenta.

4 Results and discussion

In this section we present and discuss our numerical results using the input parameters just mentioned. Returning to the energy density functional $\mathcal{E}[\rho, \tau, \vec{J}]$ in eq.(6) one observes that the expression in square brackets multiplying the kinetic energy density $\tau(\vec{r})$ has the interpretation of a reciprocal density dependent effective nucleon mass:

$$\widetilde{M}^*(\rho) = M \left[1 - \frac{5k_f^2}{28M^2} + 2M F_\tau(k_f) \right]^{-1}. \quad (31)$$

We note as an aside that this effective nucleon mass $\widetilde{M}^*(\rho)$ is conceptually different from the so-called "Landau" mass which derives from the slope of the single particle potential $U(p, k_f)$ at the Fermi surface $p = k_f$. Only if the (real) single particle potential has a simple quadratic dependence on the nucleon momentum, $U(p, k_f) = U_0(k_f) + U_1(k_f) p^2$, these two variants of effective nucleon mass agree with each other.

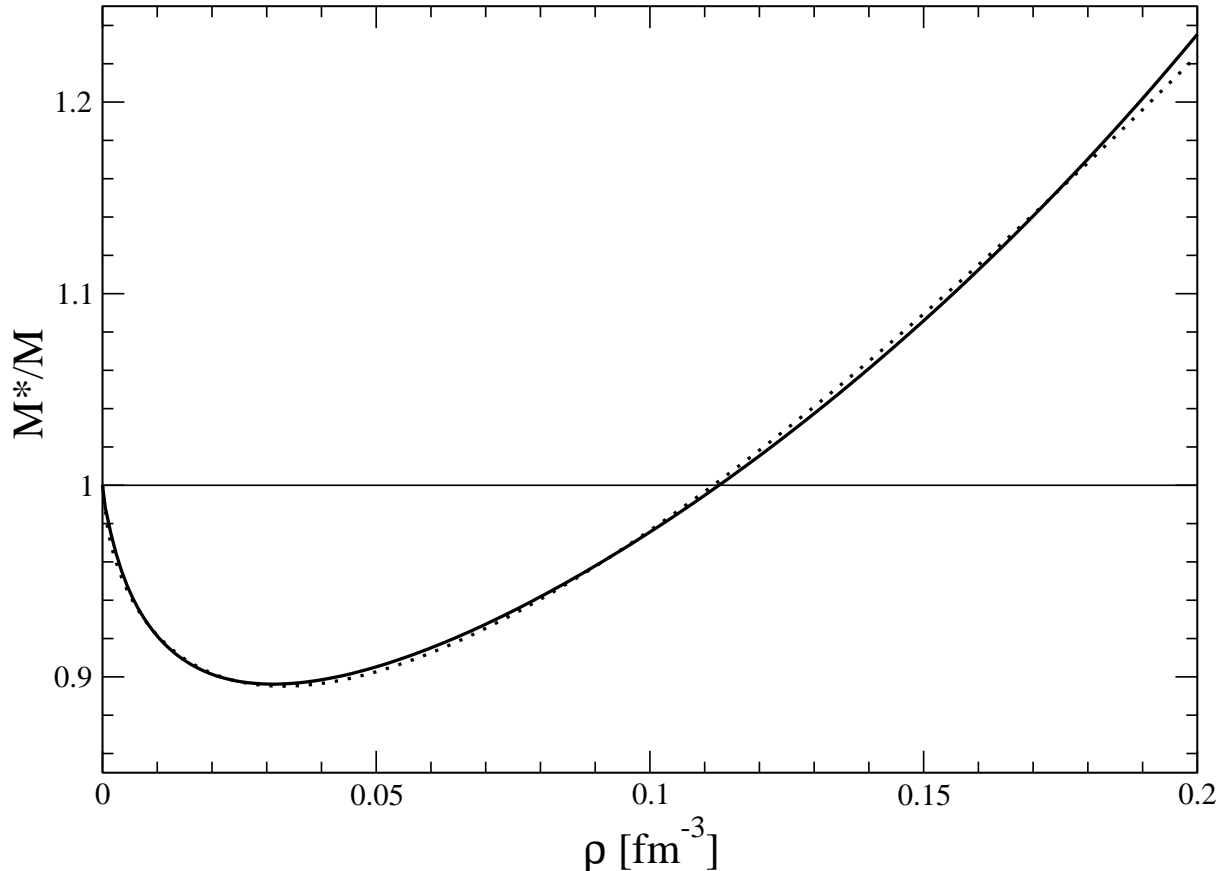


Fig. 2: The effective nucleon mass $\widetilde{M}^*(\rho)$ divided by the free nucleon mass M versus the nucleon density ρ . The dotted line corresponds to the fit: $\widetilde{M}^*(\rho)/M = 1 - 3.054 \text{ fm}^2 \cdot \rho^{2/3} + 6.345 \text{ fm}^3 \cdot \rho$.

In Fig. 2 we show the ratio effective over free nucleon mass $\widetilde{M}^*(\rho)/M$ as a function of the nucleon density $\rho = 2k_f^3/3\pi^2$. One observes a reduced effective nucleon mass $0.89M < \widetilde{M}^*(\rho) < M$ for densities $\rho < 0.11 \text{ fm}^{-3}$ and an enhanced effective nucleon mass $\widetilde{M}^*(\rho) > M$ for higher densities. In the region below the nuclear matter saturation density $\rho < \rho_0 = 0.174 \text{ fm}^{-3}$ relevant for nuclear structure the deviations of the effective nucleon mass $\widetilde{M}^*(\rho)$ from its free space value M do not exceed $\pm 15\%$. Let us give a qualitative explanation for the (somewhat unusual) behavior of the curve in Fig. 2. Consider the iterated 1π -exchange Hartree diagram in Fig. 1 at sufficiently high densities such that the pion mass m_π can be neglected against the Fermi momentum k_f . In this (limiting) case the πN -interaction vertices get cancelled by the pion propagators. One is effectively dealing with a zero-range contact interaction in second order which according to Galitskii's calculation from 1958 [13, 14] generates an enhanced in-medium mass. In this sense the curve in Fig. 2 delineates the two density regimes $k_f < \sqrt{3}m_\pi$ and $k_f > \sqrt{3}m_\pi$ where the (qualitative) behavior in the latter is ruled by Galitskii's second order result. Interestingly, a recent large scale fit of 1888 nuclide masses by Pearson et al. [15] using a "Hartree-Fock nuclear mass formula" has given an effective nucleon mass of $\widetilde{M}^*(\rho_0) = 1.05M$. This value is comparable with our parameterfree result $\widetilde{M}^*(\rho_0) = 1.15M$.

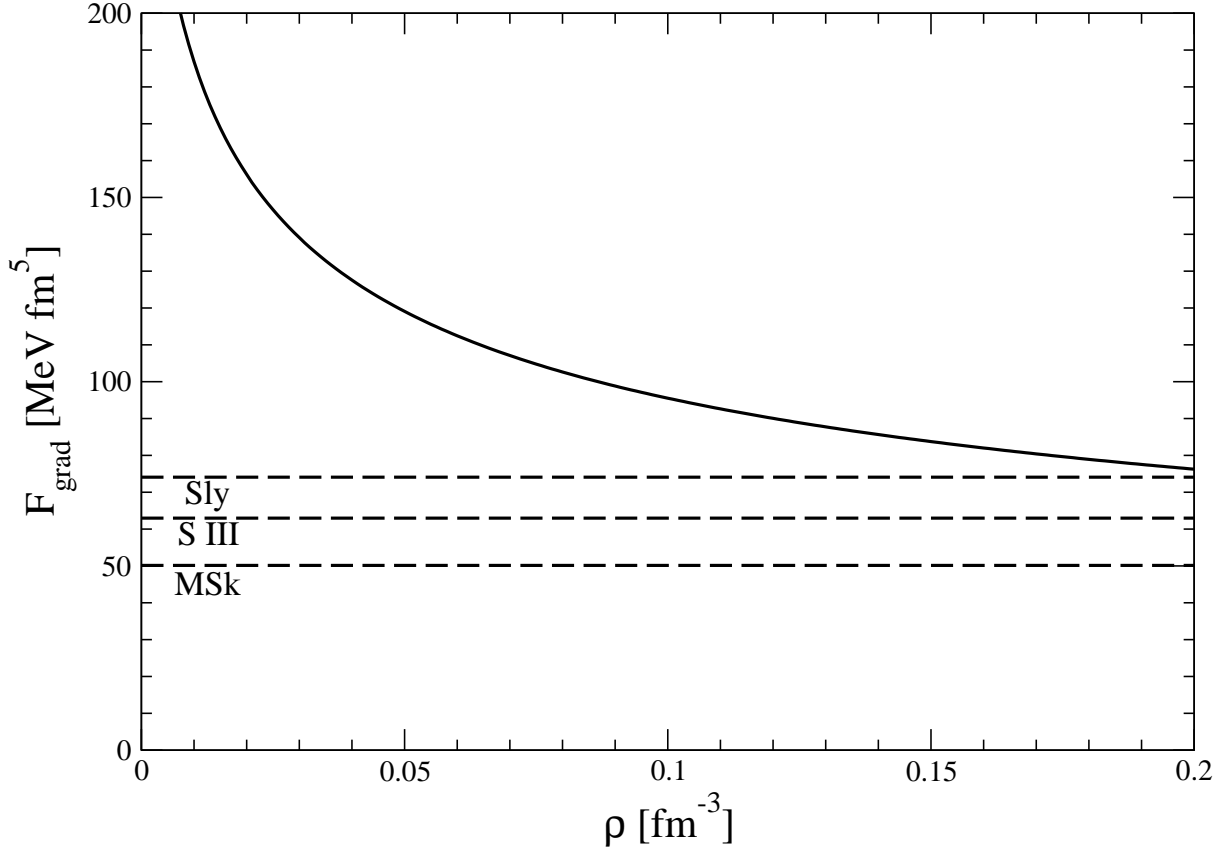


Fig. 3: The strength function $F_{\nabla}(k_f)$ related to the $(\vec{\nabla}\rho)^2$ -term in the nuclear energy density functional versus the nucleon density $\rho = 2k_f^3/3\pi^2$. An accurate fit of the full line is: $F_{\nabla}(k_f) = 45.43 \text{ MeVfm}^4 \cdot \rho^{-1/3} - 0.229 \text{ MeVfm}^2 \cdot \rho^{-1}$. The three horizontal dashed lines show the constant values $F_{\nabla}(k_f) = [9t_1 - (5 + 4x_2)t_2]/64$ of the Skyrme forces Sly [5], SIII [2] and MSk [15].

The dotted line in Fig. 2 corresponds to the fit: $\widetilde{M}^*(\rho)/M = 1 - 3.054 \text{ fm}^2 \cdot \rho^{2/3} + 6.345 \text{ fm}^3 \cdot \rho$, which may be useful for applications in nuclear structure calculations. In this context we mention also the fitted form of the underlying nuclear matter equation of state [10]: $\bar{E}(k_f) = 111.63 \text{ MeVfm}^2 \cdot \rho^{2/3} - 752.82 \text{ MeVfm}^3 \cdot \rho + 832.74 \text{ MeVfm}^4 \cdot \rho^{4/3}$.

Next, we show in Fig. 3 by the full line the strength function $F_{\nabla}(k_f)$ belonging to the $(\vec{\nabla}\rho)^2$ -term in the nuclear energy density functional eq.(6) versus the nucleon density $\rho = 2k_f^3/3\pi^2$. The three horizontal dashed lines represent the constant values $F_{\nabla}(k_f) = [9t_1 - (5 + 4x_2)t_2]/64$ of the Skyrme forces Sly [5], SIII [2] and MSk [15]. In the case of Sly and MSk we have performed averages over the various parameter sets Sly4-7 and MSk1-6. At nuclear matter saturation density $\rho_0 = 0.174 \text{ fm}^{-3}$ our parameterfree prediction $F_{\nabla}(k_{f0}) = 80.1 \text{ MeVfm}^5$ is comparable to these empirical values. The strong increase of the strength function $F_{\nabla}(k_f)$ with decreasing density has to do with the presence of a small mass scale, $m_\pi = 135 \text{ MeV}$, and with associated chiral singularities (of the form m_π^{-2} and m_π^{-1}). We will come back to this issue again towards the end of this section. An accurate fit of the full line in Fig. 3 is: $F_{\nabla}(k_f) = 45.43 \text{ MeVfm}^4 \cdot \rho^{-1/3} - 0.229 \text{ MeVfm}^2 \cdot \rho^{-1}$. It may be useful for applications in nuclear structure calculations. Note also that the relevant contribution to the central single-particle potential, $-(\vec{\nabla}\rho)^2 \partial F_{\nabla}(k_f)/\partial \rho - 2\vec{\nabla}^2 \rho F_{\nabla}(k_f)$, receives only little weight from very low densities. Therefore the deviation of the strength function $F_{\nabla}(k_f)$ from a constant may be less dramatic in practice than it appears on first sight from Fig. 3.

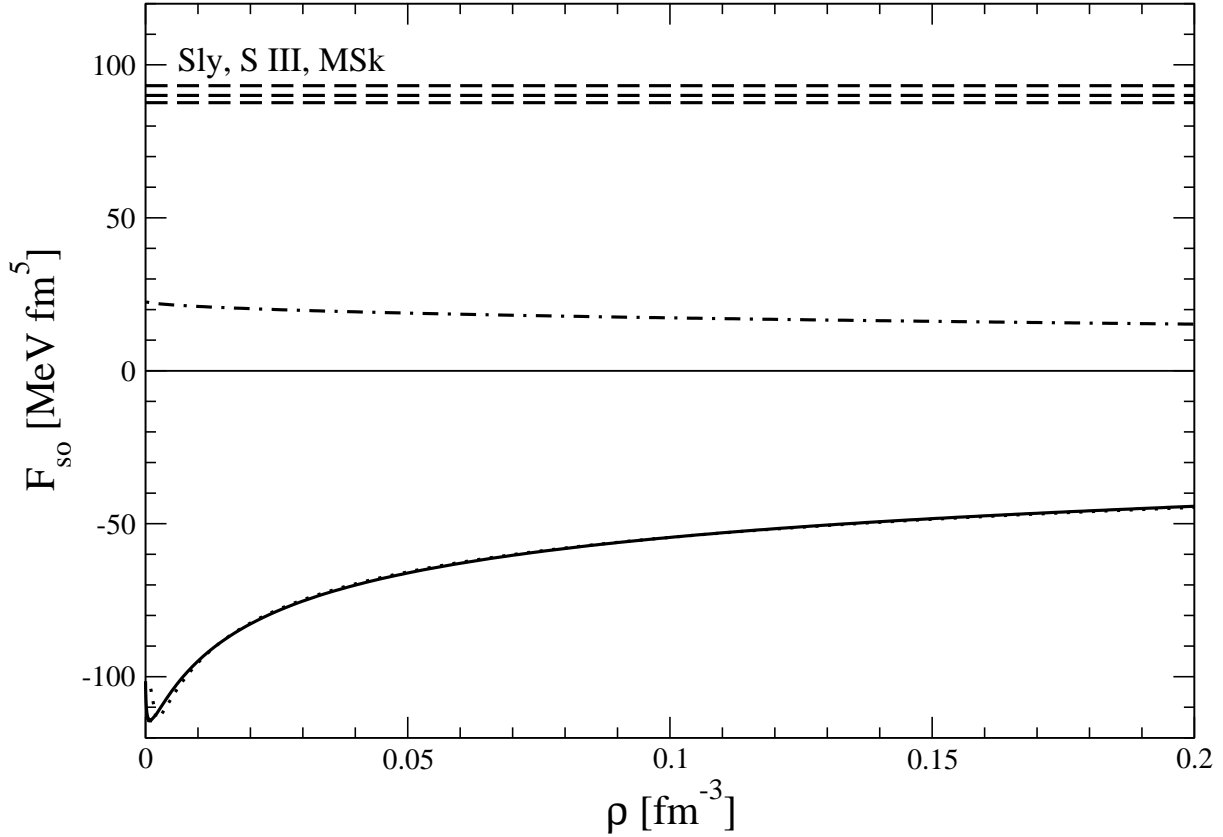


Fig. 4: The strength function $F_{so}(k_f)$ related to the spin-orbit coupling term in the nuclear energy density functional versus the nucleon density $\rho = 2k_f^3/3\pi^2$. The dotted line corresponds to the fit: $F_{so}(k_f) = 1.898 \text{ MeVfm}^3 \cdot \rho^{-2/3} - 29.37 \text{ MeVfm}^4 \cdot \rho^{-1/3}$. The three horizontal dashed lines show the constant values $F_{so}(k_f) = 3W_0/4$ of the Skyrme forces Sly [5], SIII [2] and MSk [15]. The dashed-dotted line shows the contribution from irreducible 2π -exchange written in eq.(33) for a cut-off $\Lambda = 0.65 \text{ GeV}$.

The full line in Fig. 4 shows the result of iterated 1π -exchange for the strength function $F_{so}(k_f)$ belonging to the spin-orbit coupling term in the nuclear energy density functional. For comparison we have drawn the constant values $F_{so}(k_f) = 3W_0/4$ of the three Skyrme forces Sly [5], SIII [2] and MSk [15] (horizontal dashed lines). One observes that the strength of the nuclear spin-orbit interaction as generated by iterated 1π -exchange is at ρ_0 about half as large as the corresponding empirical value, however, with the wrong negative sign. This "negative" result is dominated by the contribution of the iterated 1π -exchange Hartree diagram with two medium insertions (see eq.(13)). For example, one obtains numerically from eq.(13) at saturation density $\rho_0 = 0.174 \text{ fm}^{-3}$ (where $u = k_{f0}/m_\pi = 2.0$) the negative value $F_{so}(k_{f0}) = -83.7 \text{ MeVfm}^5$. The other diagrams with lower spin- and isospin weight factors reduce this number approximately half in magnitude. The "negative" result for $F_{so}(k_f)$ is to some extent already indicated by the calculation of the momentum and density dependent nuclear spin-orbit strength $U_{ls}(p, k_f)$ in ref.[16]. Going back to the medium insertion in eq.(5) one learns that only the values of $U_{ls}(p, k_f)$ near the Fermi surface $p = k_f$ will contribute to $F_{so}(k_f)$. As a matter of fact the curves in Fig.7 of ref.[16] drop from positive to negative values when p runs from zero to $k_{f0} = 272.7 \text{ MeV}$. Actually, for the contributions to $F_{so}(k_f)$ from diagrams with two medium insertions eqs.(13,16) the following relationship holds:

$$F_{so}(k_f) = \frac{\pi^2}{4k_f^2} \left[\frac{\partial U_{ls}(p, k_f)}{\partial k_f} + \frac{k_f}{3} \frac{\partial^2 U_{ls}(p, k_f)}{\partial p \partial k_f} \right]_{p=k_f}, \quad (32)$$

to be applied to the expressions $U_{ls}^{(a,e)}(p, k_f)$ in eqs.(9,17) of ref.[16].

It is well-known that irreducible two-pion exchange generates (via relativistic $1/M$ -corrections) spin-orbit amplitudes in the T-matrix of elastic nucleon-nucleon scattering [17]. Their effect on the nuclear spin-orbit interaction has been calculated in ref.[18]. Inserting the expression $U_{ls}^{(2\pi)}(p, k_f)$ in eq.(18) of ref.[18] into the "master formula" eq.(32) one derives the following contribution from irreducible 2π -exchange to the spin-orbit strength function:

$$F_{so}(k_f) = \frac{g_A^2}{\pi M (4f_\pi)^4} \left\{ (16 + 19g_A^2) \frac{\Lambda}{2\pi} + \frac{m_\pi^3}{6k_f^2} (4 - 3g_A^2) \ln \frac{k_f^2 + m_\pi^2}{m_\pi^2} - \frac{m_\pi}{3} (8 + 27g_A^2) + \frac{2}{3k_f} [3m_\pi^2 (g_A^2 - 2) - 4k_f^2] \arctan \frac{k_f}{m_\pi} \right\}. \quad (33)$$

Here, Λ is a momentum cut-off which has been used to regularize the linear divergences of the irreducible 2π -exchange (triangle and box) diagrams. In dimensional regularization (employed in eqs.(22,23) of ref.[17]) such linear divergences are not visible. The dashed-dotted line in Fig. 4 shows the relatively small contribution of irreducible 2π -exchange to the spin-orbit strength $F_{so}(k_f)$ for a cut-off scale of $\Lambda = 0.65$ GeV [8]. We note that without the zero-range Λ -dependent term in eq.(33) the dashed-dotted curve would be shifted downward by 45.7 MeVfm^5 to negative values.

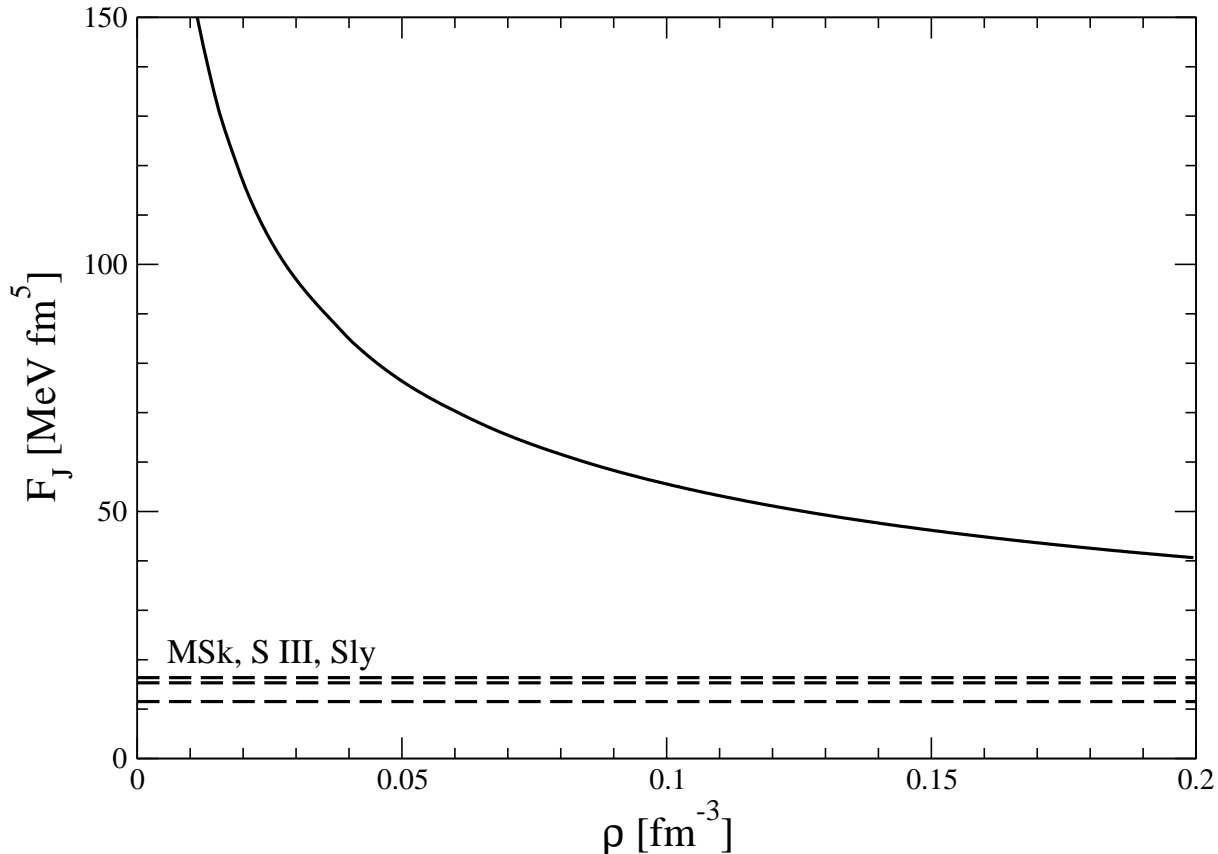


Fig. 5: The strength function $F_J(k_f)$ accompanying the squared spin-orbit density \vec{J}^2 in the nuclear energy density functional versus the nucleon density $\rho = 2k_f^3/3\pi^2$. An accurate fit of the full line is: $F_J(k_f) = 12.80 \text{ MeVfm}^{7/2} \cdot \rho^{-1/2} + 7.041 \text{ MeVfm}^4 \cdot \rho^{-1/3}$. The three horizontal dashed lines show the constant values $F_J(k_f) = [t_1(1 - 2x_1) - t_2(1 + 2x_2)]/32$ of the Skyrme forces MSk [15], SIII [2] and Sly [5].

In this context we mention also the relativistic $1/M^2$ -correction to $F_{so}(k_f)$ from the 1π -exchange Fock diagram. Inserting the expression $U_{ls}^{(1\pi)}(p, k_f)$ in eq.(6) of ref.[16] into the "master formula"

eq.(32) leads to the simple result: $F_{so}(k_f) = g_A^2[\ln(1 + 4u^2) - 4u^2]/(16Mf_\pi u)^2$, with $u = k_f/m_\pi$. As expected, this contribution with $F_{so}(2m_\pi) = -0.86 \text{ MeVfm}^5$ is negligibly small. The full line in Fig. 4 is accurately fitted by: $F_{so}(k_f) = 1.898 \text{ MeVfm}^3 \cdot \rho^{-2/3} - 29.37 \text{ MeVfm}^4 \cdot \rho^{-1/3}$.

Finally, we show in Fig. 5 the strength function $F_J(k_f)$ accompanying the squared spin-orbit density \vec{J}^2 in the nuclear energy density functional versus the nucleon density $\rho = 2k_f^3/3\pi^2$. For comparison we have drawn the constant values $F_J(k_f) = [t_1(1 - 2x_1) - t_2(1 + 2x_2)]/32$ of the three Skyrme forces MSk [15], SIII [2] and Sly [5] (dashed lines). One observes that our prediction for $F_J(k_f)$ is considerably larger. Again, there is a strong rise of the strength function $F_J(k_f)$ as one goes down to very low nucleon densities $\rho < \rho_0/10$. This time the dominant contribution comes from the iterated 1π -exchange Hartree diagram with three medium insertions eq.(21), which gives numerically at saturation density $F_J(2m_\pi) = 52.5 \text{ MeVfm}^5$. It should also be noted that the \vec{J}^2 -term in the energy density functional is often neglected in nuclear structure calculations. The full line in Fig. 5 is accurately fitted by: $F_J(k_f) = 12.80 \text{ MeVfm}^{7/2} \cdot \rho^{-1/2} + 7.041 \text{ MeVfm}^4 \cdot \rho^{-1/3}$, which may be useful for implementation into nuclear structure calculations. Note also that the \vec{J}^2 -term in the energy density functional gives rise to an additional spin-orbit single-particle field of the form $2F_J(k_f)\vec{J}$. According to our calculation this additional spin-orbit field would be rather large and strongly density dependent.

The full curves in Figs. 3,5 show a strong increase as the density ρ tends to zero. Although not visible, each curve approaches a finite value at $\rho = 0$. One can analytically derive the following low density limits:

$$\lim_{\rho \rightarrow 0} \rho^{-1} F_\tau(k_f) = \frac{3g_A^2}{(4m_\pi f_\pi)^2} \left[1 - \frac{g_A^2 M m_\pi}{128\pi f_\pi^2} \right] = 571.3 \text{ MeVfm}^5, \quad (34)$$

$$F_\nabla(0) = \frac{g_A^2}{(8m_\pi f_\pi)^2} \left[3 + \frac{59g_A^2 M m_\pi}{128\pi f_\pi^2} \right] = 339.2 \text{ MeVfm}^5, \quad (35)$$

$$F_J(0) = \frac{3g_A^2}{(4m_\pi f_\pi)^2} \left[1 - \frac{3g_A^2 M m_\pi}{256\pi f_\pi^2} \right] = 552.2 \text{ MeVfm}^5, \quad (36)$$

$$F_{so}(0) = -\frac{g_A^4 M}{\pi m_\pi (4f_\pi)^4} = -101.4 \text{ MeVfm}^5, \quad (37)$$

to which only the diagrams with two medium insertions contribute. The large numbers in eqs.(34-37) arise from negative powers of the pion mass m_π (so-called chiral singularities). The most singular m_π^{-2} -terms can be traced back to the 1π -exchange Fock diagram. It is important to keep in mind that if pionic degrees of freedom are treated explicitly in the nuclear matter problem the low density limit is realized only at extremely low densities $k_f \ll m_\pi/2$. Often, the opposite limit where the pion mass m_π can be neglected against the Fermi momentum k_f is already applicable at the moderate densities relevant for conventional nuclear physics. This is exemplified here by the approximate density dependence $F_{\nabla,so,J}(k_f) \sim k_f^{-1}$. Such a $\rho^{-1/3}$ -behavior becomes exact in the chiral limit $m_\pi = 0$ as can be deduced by simple mass dimension counting of the dominant iterated 1π -exchange diagrams (the basic argument is that $M/f_\pi^4 k_f$ has the correct unit of MeVfm^5).

5 Summary and outlook

In this work we have calculated the nuclear energy density functional $\mathcal{E}[\rho, \tau, \vec{J}]$ relevant for N=Z even-even nuclei in the systematic framework of chiral perturbation theory. Our calculation includes the 1π -exchange Fock diagram and the iterated 1π -exchange Hartree and Fock diagrams. These few leading order contributions in the small momentum expansion give already a very good

equation of state of isospin symmetric infinite nuclear matter [8, 10]. The step to inhomogeneous many-nucleon systems is done with the help of the density-matrix expansion of Negele and Vautherin [11]. Our results for the strength functions $F_\tau(k_f)$, $F_\nabla(k_f)$, $F_{so}(k_f)$ and $F_J(k_f)$ (density dependent generalizations of combinations of Skyrme force parameters) are parameterfree.

We find that the effective nucleon mass $\widetilde{M}^*(\rho)$ deviates at most by $\pm 15\%$ from its free space value M , with $0.89M < \widetilde{M}^*(\rho) < M$ for $\rho < 0.11 \text{ fm}^{-3}$ and $\widetilde{M}^*(\rho) > M$ for higher densities $\rho < \rho_0 = 0.174 \text{ fm}^{-3}$. The latter enhancement can be understood from Galitskii's second order calculation [13, 14]. Interestingly, a recent large scale fit of (almost two thousand) nuclide masses by Pearson et al. [15] finds a similarly enhanced effective nucleon mass: $\widetilde{M}^*(\rho_0) = 1.05M$.

The strength of the $(\vec{\nabla}\rho)^2$ -term, $F_\nabla(k_{f0})$, is comparable to that of phenomenological Skyrme forces. The magnitude of $F_J(k_{f0})$ accompanying the squared spin-orbit density \vec{J}^2 comes out larger.

The strength of the nuclear spin-orbit interaction, $F_{so}(k_{f0})$, as given by iterated 1π -exchange is about half as large as the corresponding empirical value $\sim 90 \text{ MeVfm}^5$, however, with the wrong negative sign. Since the (positive) contribution from irreducible 2π -exchange to $F_{so}(k_f)$ is relatively small, there remains the challenge of understanding the microscopic origin of the nuclear spin-orbit interaction. Evidently, chiral perturbation theory cannot properly account for the underlying mechanisms, whereas relativistic scalar-vector mean-field models give a successful phenomenology of the nuclear spin-orbit force. Lorentz scalar and vector mean-fields with their in-medium behavior governed by QCD sum rules could also provide the appropriate framework for that [19].

The novel density dependencies of $\widetilde{M}^*(\rho)$ and $F_{\nabla,so,J}(k_f)$ as predicted by our parameterfree calculation should be explored and examined in future nuclear structure calculations (after adding a suitable positive constant to $F_{so}(k_f)$ in order to minimally repair the spin-orbit coupling). Of course one should keep in mind that the prominent low-density behavior of $F_\nabla(k_f)$ as well as $F_J(k_f)$ carries little weight in the tails of nuclear density distributions.

For an extension to even-even nuclei with $N > Z$ the first obvious step would be to include the density dependent asymmetry energy $A(k_f)$ [8, 10] (subtracted by its kinetic energy contribution) in the nuclear energy density functional:

$$\begin{aligned} \mathcal{E}_{as}[\rho_p, \rho_n, \tau_p, \tau_n, \vec{J}_p, \vec{J}_n] &= \mathcal{E}[\rho, \tau, \vec{J}] + \mathcal{E}_{coul}[\rho_p, \tau_p, \vec{J}_p] + \frac{(\rho_n - \rho_p)^2}{\rho} \\ &\times \left\{ A(k_f) - \frac{k_f^2}{6M} + \frac{k_f^4}{12M^3} - \frac{5\tau k_f^2}{56\rho M^3} \right\} + \dots, \end{aligned} \quad (38)$$

with $\rho = \rho_p + \rho_n = 2k_f^3/3\pi^2$, $\tau = \tau_p + \tau_n$ and $\vec{J} = \vec{J}_p + \vec{J}_n$. In an ordering scheme where one counts deviations from homogeneity and deviations from isospin symmetry simultaneously as small the energy density functional in eq.(38) would already be complete. However, such a formal consideration may be too simplistic in view of neutron skins, neutron halos etc. In any case, the density-matrix expansion in eq.(1) can be straightforwardly generalized to the isospin asymmetric situation and this way the strength functions of terms like $[\tau_n - \tau_p + k_f^2(\rho_p - \rho_n)](\rho_n - \rho_p)$, $(\vec{\nabla}\rho_n - \vec{\nabla}\rho_p)^2$, $(\vec{\nabla}\rho_n - \vec{\nabla}\rho_p) \cdot (\vec{J}_n - \vec{J}_p)$ and $(\vec{J}_n - \vec{J}_p)^2$ in the nuclear energy density functional become also accessible in our diagrammatic framework. For the Coulomb energy density $\mathcal{E}_{coul}[\rho_p, \tau_p, \vec{J}_p]$ of the protons with improved treatment of the exchange (Fock) term, see ref.[20].

Acknowledgement

We thank P. Ring for suggesting this work and for useful discussions.

References

- [1] T.H.R. Skyrme, *Nucl. Phys.* **9** (1959) 615.
- [2] M. Beiner, H. Flocard, N. Van Giai and P. Quentin, *Nucl. Phys.* **A238** (1975) 29.
- [3] H. Krivine, J. Treiner and O. Bohigas, *Nucl. Phys.* **A336** (1980) 155.
- [4] J. Bartel, P. Quentin, M. Brack, C. Guet and H.-B. Hakansson, *Nucl. Phys.* **A386** (1982) 79.
- [5] E. Chabanat, P. Bonche, P. Haensel, J. Meyer and R. Schaeffer, *Nucl. Phys.* **A627** (1997) 710; **A635** (1998) 231; and references therein.
- [6] M. Bender, P.-H. Heenen and P.-G. Reinhard, "Self-Consistent Mean-Field Models for Nuclear Structure", *Rev. Mod. Phys.* **75** (2003) in print; and references therein.
- [7] P. Ring, *Prog. Part. Nucl. Phys.* **37** (1996) 193; P. Ring, Lecture Notes in Physics 581, eds. J.M. Arias and M. Lozana, Springer Verlag, (2001), page 195; and references therein.
- [8] N. Kaiser, S. Fritsch and W. Weise, *Nucl. Phys.* **A697** (2002) 255.
- [9] N. Kaiser, S. Fritsch and W. Weise, *Nucl. Phys.* **A700** (2002) 343.
- [10] S. Fritsch and N. Kaiser, nucl-th/0207057.
- [11] J.W. Negele and D. Vautherin, *Phys. Rev.* **C5** (1972) 1472.
- [12] P. Ring and P. Schuck, "The Nuclear Many-Body Problem", Springer Verlag, (1980); chapters 4 and 5.
- [13] V.M. Galitskii, *Sov. Phys.-JEPT* **7** (1958) 104.
- [14] A.L. Fetter and J.D. Walecka, "Quantum Theory of Many-Particle Systems", McGraw-Hill Inc., (1971); page 148.
- [15] J.M. Pearson, S. Goriely and M. Samyn, *Eur. Phys. J.* **A15** (2002) 13; F. Tondour, S. Goriely, J.M. Pearson and M. Onsi, *Phys. Rev.* **C62** (2000) 024308.
- [16] N. Kaiser, *Nucl. Phys.* **A709** (2002) 251.
- [17] N. Kaiser, R. Brockmann and W. Weise, *Nucl. Phys.* **A625** (1997) 758.
- [18] N. Kaiser, preprint: "Isovector nuclear spin-orbit interaction from chiral pion-nucleon dynamics".
- [19] P. Finelli, N. Kaiser, D. Vretenar and W. Weise, nucl-th/0205016.
- [20] C. Titin-Schnaider and P. Quentin, *Phys. Lett.* **B49** (1974) 397.